Infrared Physics and Technology 108 (2020) 103345

Contents lists available at ScienceDirect

Infrared Physics & Technology

journal homepage: www.elsevier.com/locate/infrared

Plasmon – Phonon interaction in $ZnSnSb_2$ + Mn semiconductors

Maja Romcevic[a,*], Novica Paunovic[a], Uros Ralevic[a], Jelena Pesic[a], Jelena Mitric[a], Jelena Trajic[a], Lukasz Kilanski[b], Witold Dobrowolski[b], Irina Valentinovna Fedorchenko[c,d], Sergey Fedorovich Marenkin[c,d], Nebojsa Romcevic[a]

[a] Institute of Physics, University of Belgrade, Belgrade, Serbia
[b] Institute of Physics, Polish Academy of Sciences, Warsaw, Poland
[c] Kurnakov Institute of General and Inorganic Chemistry, Russian Academy of Science, Moscow, Russian Federation
[d] College of New Materials and Nanotechnologies, National University of Science and Technology, Moscow, Russian Federation

ARTICLE INFO

Keywords:
Semiconductors
Lattice defects
Optical properties
Phonon properties
Plasmon - phonon interaction

ABSTRACT

Semiconductors of II-IV-V_2 type with chalcopyrite structure have been studied for several decades. Due to advances in materials synthesis technologies, and doping with various elements, the possibilities of their application have expanded. In this paper, polycrystalline $ZnSnSb_2$ + Mn was examined with the aim to explain the connection of its high free carrier concentration with the material structure and influence on optical properties. Two samples of $Zn_{1-x}Mn_xSnSb_2$ with different compositions (x = 0.027 and x = 0.076) and significant difference in carrier concentrations were analyzed. Their structural properties were examined by x-ray diffraction, optical microscopy, and AFM. The existence of several different phases - $ZnSnSb_2$, ZnSb, SnSb, and small amounts of Sn and MnSb, as well as very complex microstructures, were registered. It was found that the high free carrier concentrations are caused by a large number of defects, especially zinc vacancies. Optical properties were analyzed using IR spectroscopy at room temperature. Based on the analysis of IR reflection spectra, the presence of plasmon - phonons interaction was registered. It was determined that three $ZnSnSb_2$ phonons of B_2 symmetry interact with plasma, which then leads to the change of their positions. A detailed analysis of this interaction provides insight into the behavior of some other material parameters. Also, vibration modes of ZnSb and SnSb phases were registered on the spectra. Knowledge of phonon behavior and their interaction with plasma is important for possible applications, especially as a thermoelectric material.

1. Introduction

Semiconductors have been widely used thanks to the ability to adapt to different requirements. The II-IV-V_2 chalcopyrite semiconductors have been intensively studied in recent decades [1]. The fields of their application are considerably expanded by doping with various impurities. A significant breakthrough was achieved by the addition of magnetic impurities, whereby ferromagnetism at room temperature was achieved [2,3]. The synthesis technology of this class of compounds has been developed, but it is still adapting to new requirements [4]. Zn-Sn-Sb based alloys have required thermoelectric properties and find application as low-toxic thermoelectric materials [5,6,7]. The engineering of structural, transport, electrical, optical, magnetic properties as well as other material parameters, goes along with the increasing application of this class of semiconductors.

$ZnSnSb_2$ is II-IV-V_2 type material with the tetragonal chalcopyrite structure, narrow gap of 0.7 eV at room temperature, high concentration of free carriers (10^{21}–10^{22} cm^{-3}) and inhomogeneous structure [8,9]. In this paper we analyzed ferromagnetic semiconductor $ZnSnSb_2$ + Mn, which has interesting magnetic properties, such as paramagnet-ferromagnet transition with the Curie temperature about 522 K and the cluster-glass behavior with the transition temperature about 465 K, caused by the formation of MnSb clusters in the material [10]. The $Zn_{1-x}Mn_xSnSb_2$ samples were obtained using direct fusion method, and characterization of their structural, magnetic, optical and phonon properties were done [9]. We chose two samples with different chemical contents, x = 0.027 and x = 0.076, which we labeled as samples A and B respectively, with the aim to examine their properties in more detail. Main reason was a ten times difference in their free-carrier concentrations (p_A = 13 × 10^{21} cm^{-3} and p_B = 1.2 × 10^{21} cm^{-3}). We wanted to determine what the cause of this difference in concentration is, and whether there is a reaction between the free carriers and the crystal lattice. The question of plasmon-phonon interaction is particularly interesting in the study of thermoelectric

* Corresponding author.
E-mail address: romcevic@ipb.ac.rs (M. Romcevic).

https://doi.org/10.1016/j.infrared.2020.103345
Received 3 February 2020; Received in revised form 23 April 2020; Accepted 25 April 2020
Available online 28 April 2020
1350-4495/

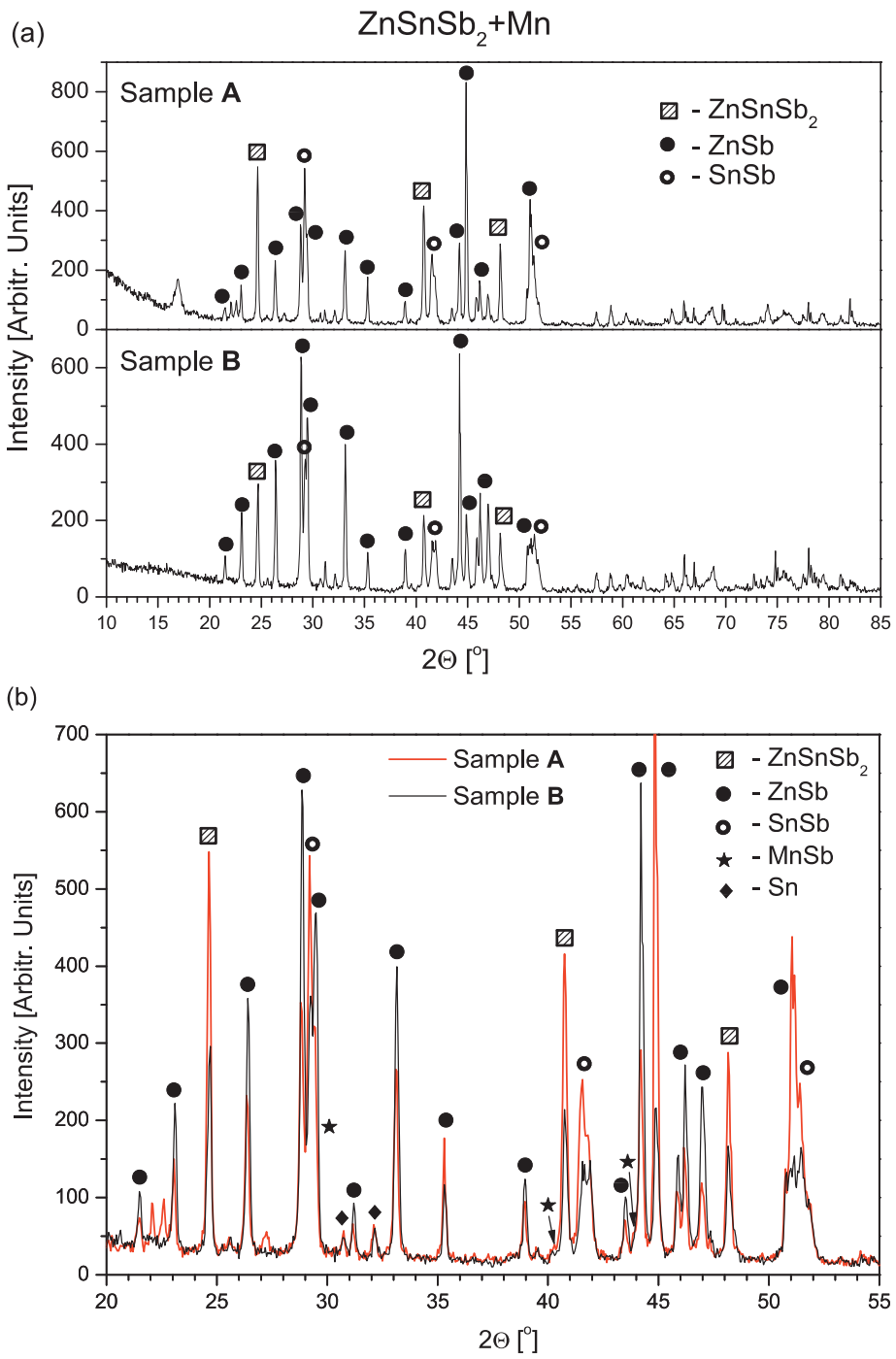

Fig. 1. (a) X-ray diffraction pattern for $ZnSnSb_2$ + Mn samples which contain different amounts of Mn. The registered crystal phases are marked; (b) The two spectra are overlapped to compare their relative intensities.

materials, as well as their electrical and thermal conductivity, and their interdependence.

$ZnSnSb_2$ is not a homogeneous material, and the consequence is that even two samples from the same crystal can have significantly different properties. This is not surprising given the complicated $ZnSnSb_2$ microstructure. Our goal was to analyze the relationship between microstructures, their phonons and free carriers, their conditionality and interactions. For this purpose we used x-ray diffraction, optical microscopy, AFM and IR spectroscopy measurements. Obtained results were analyzed by applying the model for plasmon-phonon interaction.

2. Samples and characterization

$ZnSnSb_2$ semiconductor has a chalcopyrite structure, spatial group I42d, with lattice parameters $a \approx 6.275$ Å and $c \approx 12.55$ Å and ratio c/a close to 2. $ZnSnSb_2$ melts by a peritectic reaction at $T = 362$ °C with a possible phase transformation of the cubic modification into a tetragonal one at $T = 348$ °C [11,12]. The $ZnSnSb_2$ + Mn ferromagnetic semiconductors were synthesized using the method that makes it possible to obtain single crystals at temperatures below the temperature of the peritectic reaction.

The analyzed samples of $Zn_{1-x}Mn_xSnSb_2$ were synthesized by the direct fusion method. High purity components were used for the

synthesis: zinc single crystals (99.999%), shots of tin (99.999%), antimony single crystals (99.999%), and manganese powder (99.999%). They were mixed in stoichiometric ratios.

The reaction mixture was put into a quartz glass tube and heated up to 631 °C. After that, ampoules were quenched to 355 °C and then annealed at 355 °C. This is described in more detail in the papers [12,13]. The synthesized crystals were cut into slices of about 1.5 mm thickness.

The chemical composition of the samples (x) was determined using the energy dispersive x-ray fluorescence method (EDXRF) [10]. Obtained results showed that average Mn content (x) in the samples is between 0.027 and 0.138. All the studied crystals had the correct stoichiometry of $Zn_{1-x}Mn_xSnSb_2$ alloy equal to 1-x : x : 1 : 2, within our measurement accuracy of about 10% of the x value.

Based on the magnetotransport measurements [10] it was found that electrical and magnetotransport parameters, such as resistivity, carrier concentration, and carrier mobility, do not depend linearly on composition, i.e. on the Mn content. Therefore, as mentioned above, two samples with a considerable difference in free-carrier concentrations were selected. The sample with $x = 0.027$ and $p = 13 \times 10^{21}$ cm^{-3} was labeled as sample A and the one with $x = 0.076$ and $p = 1.2 \times 10^{21}$ cm^{-3} as sample B. In this way we wanted to determine the connection between the free carriers and the structural and optical properties of the alloy.

The structural properties of these samples were investigated by the XRD powder technique. Measurements were done using a Philips PW 1050 diffractometer equipped with a PW 1730 generator, 40 kV × 20 mA, using Ni filtered Co Ka radiation of 0.1778897 nm at room temperature. The x-ray diffraction patterns were collected during 2 h in the range of $10-100^{\circ}$ with a scanning step of 0.05° and 10 s scanning time per step. Phase analysis showed that besides the main phase of chalcopyrite $ZnSnSb_2$, the orthorhombic ZnSb, rhombohedral SnSb, and hexagonal MnSb phases are present in the samples. This is consistent with the literature [8,10].

An optical microscope was used to get an insight into the distribution of different phases of the material along the surface. Images were captured using Olympus BH series modular microscope with UIS objective lenses with 50x and 400x enhancement.

The surfaces of $ZnSnSb_2$ + Mn samples were examined in detail using Atomic Force Microscope (AFM), NTEGRA prima from NTMDT. The topography and phase images were acquired simultaneously by operating the AFM in semi-contact mode. NSG01 probes with a typical resonant frequency of 150 kHz and 10 nm tip apex curvature radius were used.

The far-infrared (FIR) reflectivity measurements were done with a BOMEM DA-8 Fourier-transform infrared spectrometer in the spectral range from 40 to 450 cm^{-1} at room temperature. A Hyper beamsplitter and deuterated triglycine sulfate (DTGS) pyroelectric detector were used.

3. Results and discussion

It is known that during the preparation of $ZnSnSb_2$ the polycrystalline material is formed, consisting of the main phase and ZnSb, SnSb and β-Sn inclusions [11].

The structure of the two selected samples was investigated by X-ray diffraction measurements. Obtained results with marked phases are presented in Fig. 1. In Fig. 1(b) the overlap of the results is shown, with the aim to compare their relative intensities. The list of XRD peaks positions and their corresponding Miller indices and phases is given in Table 1 in Supplementary Materials.

Besides the chalcopyrite $ZnSnSb_2$ phase the orthorhombic ZnSb, rhombohedral SnSb, Sn have also been registered, as well as weak lines from hexagonal MnSb inclusions. The idea was to detect differences in the structures of these two samples. It is obvious that diffraction lines corresponding to the $ZnSnSb_2$ phase (squares) are stronger for sample A as well as lines of SnSb phase (open circles). Also, it is clear that lines corresponding to ZnSb (black circles) are mostly stronger for sample B. Existence of the Sn phase is evident, but lines corresponding MnSb phase are barely visible.

Table 1
Expected values of $ZnSnSb_2$ phonons of B_2 and E symmetries, from literature [26].

Phonon	B_2^1	B_2^2	B_2^3	E^1	E^2	E^3	E^4	E^5	E^6
Estimated value [cm^{-1}]	189	199	70	189	185	195	111	88	54

In order to examine the spatial distribution of the existing different crystal phases, the samples were recorded by an optical microscope with two different magnifications (50 × and 400 ×). Obtained micrographs are presented in Fig. 2.

Existing phases are clearly visible and they form multiphase structures. It should be noted that this is a very non-homogeneous material and that images from different parts of the samples differed, so the characteristic ones are selected and shown in Fig. 2.

In our previous work [9] is determined that gray fields are $ZnSnSb_2$ crystal, white ones correspond SnSb phase and that dark parts consist of ZnSb. Micrometric crystals of MnSb in the shape of dark circles were registered also.

Although microstructures of similar shapes have been formed in both samples, it is apparent that the surfaces significantly differ. Based on previous work [8,9,14], it can be concluded that these spherical and needle like microcrystals are ZnSb, MnSb, Sn, and Sb phases formed during crystallization of the material. As can be seen from Fig. 2. the sample B contains a lot of micron-sizes phases relatively evenly distributed over the surface (volume).

In order to more accurately examine the surface of the samples, we used atomic force microscopy (AFM) measurements. The characteristic results are presented in Fig. 3.

The surfaces of both samples have a granular structure. The sample A has evenly distributed grains over the entire surface with a few larger clusters and an average grain height of around ~100 nm (see Fig. 3(a) and the profile in Fig. 3(c)). The phase contrast in Fig. 3(b) originates exclusively from the abrupt changes in the height, indicating that the material properties of the sample A surface are homogeneous. The grains on the surface of the sample B are exclusively arranged into clusters which are not evenly distributed over the surface. The majority of the clusters reach several tens of nm in height, with a few exceptions having a height of ~100 nm (see Fig. 3(d) and the profile in Fig. 3(f)). The phase contrast of the sample B surface shows that the larger clusters have a distinct phase shift, seen as dark and white regions in Fig. 3(e), so that clusters have different material properties than the remainder of the surface.

This material is known to be difficult to synthesize and beside $ZnSnSb_2$ the ZnSb and SnSb phases are formed [11,15]. The series of $Zn_{1-x}Mn_xSnSb_2$ samples were synthesized under the same conditions with the only difference being the starting amounts of manganese and zinc [10]. Obviously, the small variation in the starting mixture causes rather different structures and properties of the materials.

It was found that a large concentration of lattice defects, especially in the cation sublattice, in $ZnSnSb_2$, as well as in other II-IV-V_2 semiconductors [16,17], causes a high hole concentration. In particular, Zn vacancies are those defects that lead to a very high concentration of holes [18,19,20]. Typical hole concentration in $ZnSnSb_2$ is 10^{20} cm^{-3} [15–20], in two-component p-type ZnSb it is 10^{19} cm^{-3} [18,19], while SnSb is a n-type material with metallic character and electron concentration of about 10^{22} cm^{-3} at 1.8 K [21]. Evidently, the electronic structure is very complex in this material.

It is difficult to say exactly what is the cause of different hole concentrations in the $Zn_{1-x}Mn_xSnSb_2$ samples, but it could be assumed that Zn vacancies are the main reason. Sample A has a higher content of

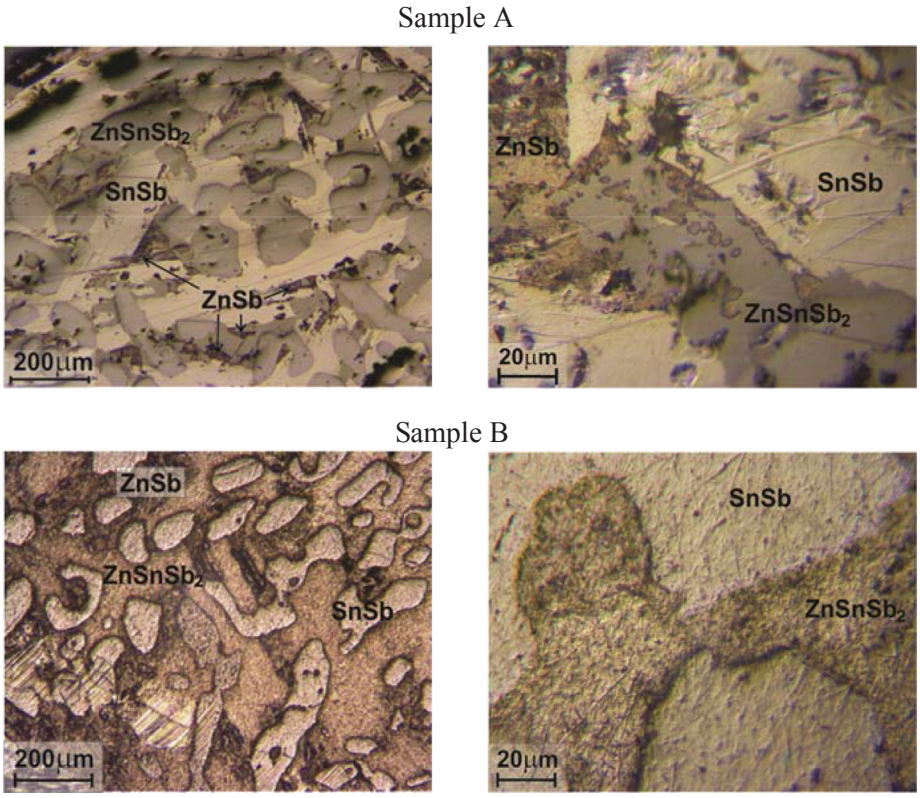

Fig. 2. Micrographs of the $ZnSnSb_2$ + Mn samples surfaces with magnifications of 50 × and 400×.

SnSb, which is related to a higher deficiency of Zn atoms, and therefore higher hole concentration. So, the different concentrations of free carriers in the samples are a consequence of various defects and microstructures which are formed.

In order to examine the interaction of free carriers and a lattice, the far-infrared reflectivity spectra in the range 40–450 cm^{-1} at room temperature have been recorded. Obtained spectra are shown in Fig. 4.

It is obvious that the most distinct difference between the spectra relates to wave numbers above 220 cm^{-1}, where the high carrier concentration has a main influence. Also, in the range from 120 to 180 cm^{-1} the spectrum for sample B (black line) contains some phonon lines which are absent or attenuated in the spectrum for sample A (red line).

A detailed analysis of the obtained results was necessary. For the analysis of the spectra the fitting procedure which includes plasmon - phonon interaction was applied.

4. Plasmon - phonon interaction

In materials with high free carrier concentration a plasmon-phonon interaction should be taken into account, as it significantly affects the properties of the material. Its influence on the dielectric properties of the material is important for the analysis of the reflection spectra.

A theoretical model of the dielectric function in bulk materials [22] has been applied. The dielectric function $\varepsilon(\omega)$ describes dielectric properties of single crystal and includes classical oscillators corresponding to the TO-modes, and Drude part which takes into account the free carrier contribution:

$$\varepsilon(\omega) = \varepsilon_\infty + \sum_{k=1}^{l} \frac{\varepsilon_\infty(\omega_{LOk}^2 - \omega_{TOk}^2)}{\omega_{TOk}^2 - \omega^2 - i\gamma_{TOk}\omega} - \frac{\varepsilon_\infty \omega_P^2}{\omega(\omega + i\Gamma_P)} \quad (1)$$

In this equation ε_∞ is the high-frequency dielectric constant, ω_{TOk} and ω_{LOk} are the transverse and longitudinal optical-phonon frequencies, l is the number of phonons,ω_P is the plasma frequency, γ_{TOk} and Γ_P are the phonon and plasmon damping. The use of such a dielectric function is valid in multiphase materials, since it is based on a phenomenological approach where the effective values of the material parameters are used, e.g. $\omega_p^2 = \omega_{p1}^2 + \omega_{p2}^2 + \omega_{p3}^2 + \cdots$.

As our $ZnSnSb_2$ + Mn samples have high concentration of free-carriers (p), and therefore high values of ω_P ($\omega_P{}^2 \sim p$), it is expected that plasma interacts with phonons. As a result the phonon frequencies are changed, i.e. their positions are shifted from the expected values. The phonon lines observed at the reflection spectra are these shifted modes i.e. coupled plasmon-phonon modes. So, the situation is much clearer if the dielectric function which takes a plasmon–phonon interaction in advance is used [23,24]. It also allows the possibilities that more than one phonon interact with plasma as well as existence of uncoupled phonons. That dielectric function is:

$$\varepsilon(\omega) = \varepsilon_\infty \frac{\prod_{j=1}^{n+1}(\omega^2 + i\gamma_{lj}\omega - \omega_{lj}^2)}{\omega(\omega + i\Gamma_P)\prod_{i=1}^{n}(\omega^2 + i\gamma_{ti}\omega - \omega_{ti}^2)} \cdot \prod_{k=1}^{s} \frac{\omega^2 + i\gamma_{LOk}\omega - \omega_{LOk}^2}{\omega^2 + i\gamma_{TOk}\omega - \omega_{TOk}^2} \quad (2)$$

The first fraction in Eq. (2) describes coupling of a plasmon and n LO phonons, where parameters ω_{lj} and γ_{lj} are eigenfrequencies and damping coefficients of the longitudinal component of the coupled phonons. ω_{ti} and γ_{ti} are frequencies and damping of transverse component of these phonons. Γ_p is the plasma damping. The second factor in Eq. (2) represents s uncoupled phonons of the crystal, wherein ω_{LOk} (ω_{TOk}) and γ_{LOk} (γ_{TOk}) are LO (TO) frequencies and damping coefficients of the k-th uncoupled phonon of the crystal.

The analysis of the obtained reflection spectra was performed by a fitting procedure, by adjusting the parameters of Eq. (2) in order to obtain a match between the experimental and theoretical curves. The values of ω_{lj} and ω_{ti} are directly obtained in this way while the ω_P and ω_{LO} values are calculated [25]. It can be seen that the positions of the ω_{l2} and ω_{l4} are significantly different for samples A and B. The behavior of phonons and interactions with plasma were analyzed based on the data thus obtained.

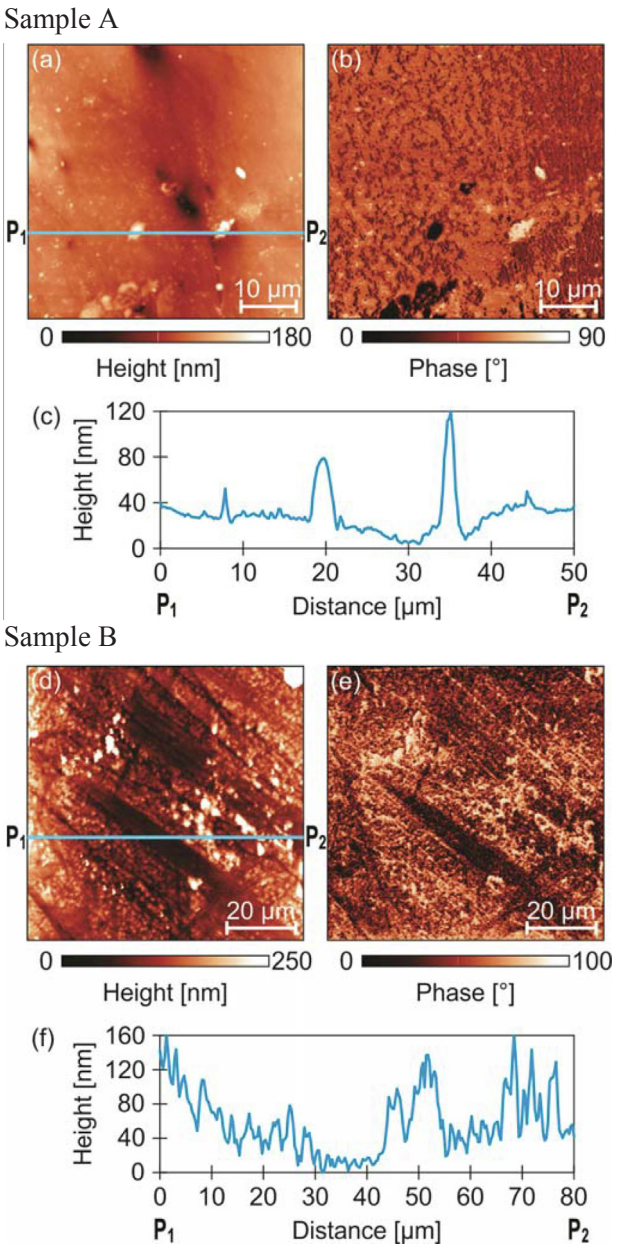

Fig. 3. (a) AFM topography and (b) corresponding phase-contrast image of sample A; (c) Height profile taken along the straight solid line in (a) from point P_1 to point P_2; Figures (d), (e), and (f) refer to sample B in the same way.

The phonons of $ZnSnSb_2$ which are IR active are known from literature [26], and they are of B_2 and E symmetries. Their estimated values are given in Table 1.

Plasmon - phonon interaction commonly refers to the coupling of the plasma and one phonon [27]. In that case two coupled modes appear ω_{l1} and ω_{l2}, often labeled as ω_+ and ω_-. In the case of $ZnSnSb_2$, based on data obtained by fitting procedure, it was established that the plasma interacts with three phonons of B_2 symmetry [28,29,30]. As a result of that their positions are shifted and instead three B_2 modes there are four coupled modes ω_{l1}, ω_{l2}, ω_{l3} and ω_{l4}. Obtained values are shown as black points in Fig. 6. Their positions are different for the two samples because of the different influences of the plasma ($\omega_P^2 \sim p$). Because of the high plasma frequency of sample A, the ω_{l4} has high value of 675 cm^{-1} which is outside of the measured range.

For ease of analysis, it is common to draw a dependency diagram of obtained parameters (ω_{lj}, ω_t, ω_{TO}, ω_{LO}) on plasma frequency ω_p, as

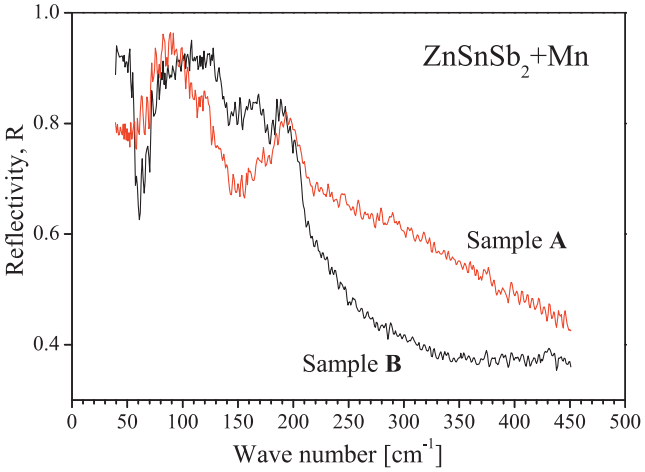

Fig. 4. Far-infrared reflectivity spectra of $ZnSnSb_2$ + Mn.

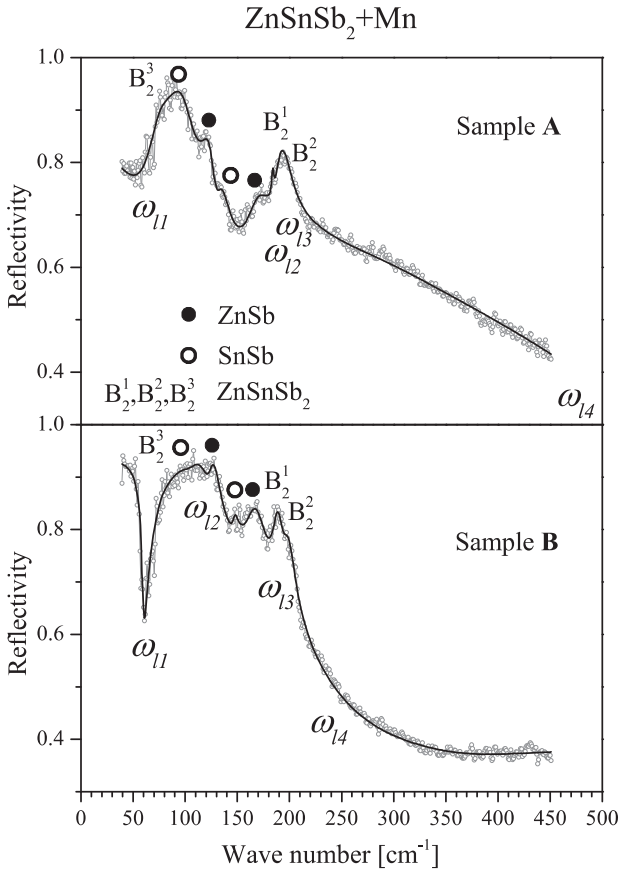

Fig. 5. Analyzed reflection spectra; experimental data are represented by circles while black lines are theoretical curves; registered optical phonons are indicated on the spectra.

shown in Fig. 6. The full lines are solutions of $Re\{\varepsilon(\omega)\} = 0$ from Eq. (1). It should be noted that line ω_{l3} between B_2^1 and B_2^2 phonons is barely visible because they are very close. The lines are calculated for five different values of plasma damping Γ_p (Fig. 6) ($\Gamma_p = 1/\tau$, where τ is a lifetime of plasmon). This was done to determine Γ_p interdependence with plasmon - phonon interaction.

The obtained values of plasma damping and plasma frequency of samples A and B are: $\Gamma_{pA} = 500$ cm^{-1}, $\Gamma_{pB} = 375$ cm^{-1}, $\omega_{pA} = 837$ cm^{-1} and $\omega_{pB} = 405$ cm^{-1}. It should be noted that these parameters represent the effective values that describe the sample as a

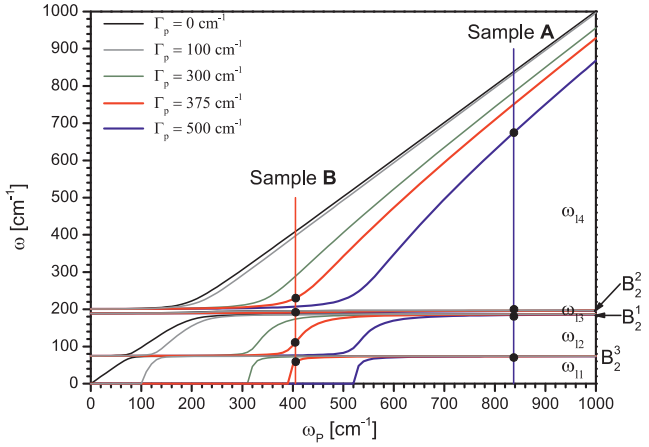

Fig. 6. Analysis of plasmon - three-phonons interaction; Full lines are obtained from Eq.(1), as the solutions of Re{$\varepsilon(\omega)$} = 0, for various values of Γ_p; Black points represent experimentally obtained data for ω_{lj} for both samples (Eq. (2)).

whole. It could be expected (based on p_A and p_B values and $\omega_p^2 \sim p$) that ω_{pA} and ω_{pB} differ about three times, which was not established. Plasma frequency is defined as $\omega_p^2 = (n_p e^2)/(\varepsilon_0 \varepsilon_\infty m_h^*)$, i.e. it includes other parameters of the material. Thus, by determining the plasma frequency and plasma damping the other properties of the material can be analyzed.

Besides phonons of B_2 symmetry which interact with plasma, other $ZnSnSb_2$ phonons are not registered on the IR reflectivity spectra. However, characteristic phonons of the other phases can be identified, as can be seen in Fig. 5. It was necessary that these phonons are not covered by the plasmon - phonon interaction. ZnSb modes are noticed at about 125 and 165 cm^{-1}, which is in agreement with results from the literature [31]. Two modes that correspond to SnSb phase are at about 94 and 145 cm^{-1}, which matches the previously obtained data [9,32]. The appearance of these modes is expected due to the significant presence of ZnSb and SnSb phases in the samples. MnSb phonons are not registered, i.e. it was not possible to discern them due to the small amount of that phase.

Based on the performed analyses, it can be seen that different microstructures formed in the investigated samples lead to high concentrations of free carriers, but which are ten times different from each other. Those high values cause plasmon - B_2 phonons interaction. That can be used to analyze optical and electrical properties of the materials, as well as other parameters, such as dielectric constants, effective mass of charge carriers and phonon lifetimes. In this way, the multiphase material with different microstructures was analyzed as a whole.

Investigation of thermoelectric properties of $ZnSnSb_2$ is a current issue [5,15,33]. The analysis of plasmon - phonon interaction performed in this paper can significantly assist in the study and understanding of thermoelectric processes in this as in other semiconducting polycrystalline materials [34].

5. Conclusion

Two samples of $ZnSnSb_2$ + Mn with different amounts of manganese were analyzed in this paper. The small difference in the initial composition of the material led to a difference of ten times in the free carrier concentrations. Their structural properties were examined by x-ray diffraction, optical microscopy, and AFM. Several different phases were registered - $ZnSnSb_2$, ZnSb, SnSb, and small amounts of Sn and MnSb. These phases form different microstructures, which is related to the large irregularities of the lattice. It was found that the high free carrier concentrations are caused by a large number of defects, especially zinc vacancies.

The optical characteristics of these multiphase materials were examined, whereby the samples were considered as a whole. Based on the analysis of IR reflection spectra the presence of a plasmon - phonons interaction was confirmed. It was determined that three $ZnSnSb_2$ phonons of B_2 symmetry interact with plasma, which led to the change of their positions. It is clear that strong plasmon - phonon interaction modifies optoelectronic properties of the $ZnSnSb_2$ + Mn samples, and that phonon positions depend on a free carrier concentration. A detailed analysis of this interaction also provides insight into the behavior of other material parameters, such as dielectric constants, effective mass of charge carriers and phonon lifetimes. Also, vibration modes of ZnSb and SnSb phases were registered on the spectra. Knowledge of phonon behavior in a material, as well as interaction with plasma, is very important for studying its thermoelectric properties.

Declaration of competing interest

The authors declare that there is no conflict of interest in this paper.

Acknowledgement

This work was supported under the Agreement of Scientific Collaboration between Polish Academy of Science and Serbian Academy of Sciences and Arts. The work in Serbia was supported by the Serbian Ministry of Education, Science and Technological Development through Project 45003.

Appendix A. Supplementary material

Supplementary data to this article can be found online at https://doi.org/10.1016/j.infrared.2020.103345.

References

[1] J.L. Shay, J.H. Wernick, Ternary Chalcopyrite Semiconductors: Growth, Electronic Properties, and Applications, Chapter 3 - Electronic Structure of II-IV-V_2 Compounds, Pergamon Press, New York, 1975, pp. 79–109 https://doi.org/10.1016/B978-0-08-017883-7.50008-1.
[2] W. Dobrowolski , J. Kossut, T. Story. II–VI and IV–VI Diluted Magnetic Semiconductors – New Bulk Materials and Low-Dimensional Quantum Structures. Handbook of Magnetic Materials 15 (2003) pp. 289-377, (Elsevier, Amsterdam, 2003). https://doi.org/10.1016/S1567-2719(03)15003-2.
[3] L. Kilanski, M. Górska, W. Dobrowolski, E. Dynowska, M. Wójcik, B.J. Kowalski, J.R. Anderson, C.R. Rotundu, D.K. Maude, S.A. Varnavskiy, I.V. Fedorchenko, S.F. Marenkin, Magnetism and magnetotransport of strongly disordered $Zn_{1-x}Mn_xGeAs_2$ semiconductor: The role of nanoscale magnetic clusters, J. Appl. Phys. 108 (2010) 073925, , https://doi.org/10.1063/1.3490231.
[4] S.F. Marenkin, A.D. Izotov, I.V. Fedorchenko, V.M. Novotortsev, Manufacture of magnetic granular structures in semiconductor-ferromagnet systems, Russ. J. Inorg. Chem. 60 (2015) 295300, , https://doi.org/10.1134/S0036023615030146.
[5] M. Ito, Y. Ohishi, H. Muta, K. Kurosaki, S. Yamanaka, Thermoelectric properties of Zn-Sn-Sb based alloys, Mater. Res. Soc. Symp. Proc. 1314 (2011), https://doi.org/10.1557/opl.2011.618.
[6] P. Balasubramanian, M. Battabyal, D. Sivaprahasam, R. Gopalan, On the formation of phases and their influence on the thermal stability and thermoelectric properties of nanostructured zinc antimonide, J. Phys. D: Appl. Phys. 50 015602 (11 (2017) pp), https://doi.org/10.1088/1361-6463/50/1/015602.
[7] G. Coquil, B. Fraisse, S. Biscaglia, D. Ayme-Perrot, M.T. Sougrati, L. Monconduit, $ZnSnSb_2$ anode: A solid solution behavior enabling high rate capability in Li-ion batteries, J. Power Sour. 441 (2019) 227165, , https://doi.org/10.1016/j.jpowsour.2019.227165.
[8] O. Zobac, J. Sopousek, J. Bursik, A. Zemanova, P. Roupcova, Experimental Study of the Sb-Sn-Zn Alloy System, Metall. Mater. Trans. 45A (2014) 1181–1188, https://doi.org/10.1007/s11661-013-2104-1.
[9] M. Romcevic, M. Gilic, L. Kilanski, W. Dobrowolski, I.V. Fedorchenko, S.F. Marenkin, N. Romcevic, Phonon properties of $ZnSnSb_2$ + Mn semiconductors: Raman spectroscopy, J. Raman Spectrosc. 49 (2018) 1678–1685, https://doi.org/10.1002/jrs.5421.
[10] L. Kilanski, M. Gorska, A. Slawska-Waniewska, S. Lewinska, R. Szymczak, E. Dynowska, A. Podgorni, W. Dobrowolski, U. Ralevic, R. Gajic, N. Romcevic, I.V. Fedorchenko, S.F. Marenkin, High temperature magnetic order in Zn_{1-x} Mn $_x$ $SnSb_2$ + MnSb nanocomposite ferromagnetic semiconductors, J. Phys.:Condens. Matter. 28 (2016) 336004, , https://doi.org/10.1088/0953-8984/28/33/336004.
[11] A. Tenga, F.J. Garcia-Garcia, A.S. Mikhaylushkin, B. Espinosa-Arronte, M. Andersson, U. Haussermann, Sphalerite – Chalcopyrite Polymorphism in Semimetallic $ZnSnSb_2$, Chem. Mater. 17 (2005) 6080–6085, https://doi.org/10.

1021/cm0516053.
[12] A. Tenga, F.J. Garcia-Garcia, Y. Wu, N. Newman, U. Haussermann, Metal-nonmetal transition in the sphalerite-type solid solution $[ZnSnSb_2]_{1-x}[2(InSb)]_x$, J. Solid State Chem. 182 (2009) 1438–1442, https://doi.org/10.1016/j.jssc.2009.03.015.
[13] M. Bostrom, S. Hovmoller, Preparation and Crystal Structure of the Pseudo-Decagonal Approximant Mn_3Ga_5, J. Solid State Chem. 153 (2000) 398–403, https://doi.org/10.1006/jssc.2000.8790.
[14] C. Wang, Y. Xu, S. Yang, H. Jiang, J. Li, J. Zhu, S. Yang, X. Liu, Experimental Determination of Phase Equilibria in the Sn-Zn-Sb System, J. Phase Equil. Diff. 36 (2015) 350–356, https://doi.org/10.1007/s11669-015-0387-1.
[15] A. Nomura, S. Choi, M. Ishimary, A. Kosuga, T. Chasapis, S. Ohno, G.J. Snyder, Y. Ohishi, H. Muta, S. Yamanaka, K. Kurosaki, Chalcopyrite $ZnSnSb_2$: A Promising Thermoelectric Material, ACS Appl. Mater. Interf. 10 (2018) 43682–43690, https://doi.org/10.1021/acsami.8b16717.
[16] V.N. Brudnyi, Electronic properties and pinning of the Fermi level in irradiated II–IV–V_2 semiconductors, Semiconductors 43 (2009) 1146–1154, https://doi.org/10.1134/S1063782609090085.
[17] V.G. Voevodin, S.N. Grinyaev, O.V. Voevodina, Nonstoichiometry and point defects in nonlinear optical crystals $A^2B^4C_2^5$, Mater. Sci. Semicond. Proces. 6 (2003) 385–388, https://doi.org/10.1016/j.mssp.2003.07.006.
[18] X. Song, M. Schrade, N. Maso, T.G. Finstad, Zn vacancy formation, Zn evaporation and decomposition of ZnSb at elevated temperatures: Influence on the microstructure and the electrical properties, J. Alloys Comp. 710 (2017) 762–770, https://doi.org/10.1016/j.jallcom.2017.03.339.
[19] L.V. Prokofieva, P.P. Konstantinov, A.A. Shabaldin, On the tin impurity in the thermoelectric compound ZnSb: Charge-carrier generation and compensation, Semicond 50 (2016) 741–750, https://doi.org/10.1134/S1063782616060208.
[20] L. Bjerg, G.K.H. Madsen, B.B. Iversen, Ab initio Calculations of Intrinsic Point Defects in ZnSb, Chem. Mater. 24 (2012) 2111–2116, https://doi.org/10.1021/cm300642t.
[21] B. Liu, J. Wu, Y. Cui, H. Wang, Y. Liu, Z. Wang, Z. Ren, G. Cao, Superconductivity in SnSb with a natural superlattice structure, Supercond. Sci. Technol. 31 (2018) 7, https://doi.org/10.1088/1361-6668/aae6fe 125011.
[22] Abstreiter G., Cardona M., Pinczuk A. Light scattering by free carrier excitations in semiconductors. In: Cardona M., Güntherodt G. (eds) Light Scattering in Solids IV. Topics in Applied Physics, vol 54. Springer, Berlin, Heidelberg. (1984) https://doi.org/10.1007/3-540-11942-6_20.
[23] A.A. Kukharskii, Plasmon-phonon coupling in GaAs, Solid State Commun. 13 (1973) 1761–1765, https://doi.org/10.1016/0038-1098(73)90724-2.
[24] N. Romcevic, M. Romcevic, W.D. Dobrovolski, L. Kilanski, M. Petrovic, J. Trajic, B. Hadzic, Z. Lazarevic, M. Gilic, J.L. Ristic-Djurovic, N. Paunovic, A. Reszka, B.J. Kowalski, I.V. Fedorchenko, S.F. Marenki, Far-infrared spectroscopy of Zn1 − xMnxGeAs2 single crystals: Plasma damping influence on plasmon – Phonon interaction, J. Alloys Comp. 649 (2015) 375–379, https://doi.org/10.1016/j.jallcom.2015.07.087.
[25] J. Trajic, N. Romcevic, M. Gilic, M. Petrovic Damjanovic, M. Romcevic, V.N. Nikiforov, Optical properties of $PbTe_{0.95}S_{0.05}$ single crystal at different temperatures: Far - infrared study, Optoelec. Adv. Mater. Rap. Comm. 6 (2012) 543–546.
[26] F.W. Ohrendorf, H. Haeuseler, Lattice Dynamics of Chalcopyrite Type Compounds. Part I. Vibrational Frequencies, Cryst. Res. Technol. 34 (1999) 339–349, https://doi.org/10.1002/(SICI)1521-4079(199903)34:3<339:: AID-CRAT339>3.0.CO;2-E.
[27] Klein M.V. Electronic Raman Scattering. In: Cardona M. (eds) Light Scattering in Solids. Topics in Applied Physics, vol 8. Springer, Berlin, Heidelberg (1975). https://doi.org/10.1007/978-3-540-37568-5_4.
[28] M. Petrovic, N. Romcevic, J. Trajic, W.D. Dobrowolski, M. Romcevic, B. Hadzic, M. Gilic, A. Mycielski, Far-infrared spectroscopy of $CdTe_{1-x}Se_x$(In): Phonon properties, Infrared Phys. Tech. 67 (2014) 323–326, https://doi.org/10.1016/j.infrared.2014.08.010.
[29] M. Romcevic, N. Romcevic, W. Dobrowolski, L. Kilanski, J. Trajic, D.V. Timotijevic, E. Dynowska, I.V. Fedorchenko, S.F. Marenkin, Optical properties and plasmon – Two different phonons coupling in ZnGeAs2 + Mn, J. Alloys Comp. 548 (2013) 33–37, https://doi.org/10.1016/j.jallcom.2012.09.017.
[30] I.J. Luxmoore, C.H. Gan, P.Q. Liu, F. Valmorra, P. Li, J. Faist, G.R. Nash, Strong coupling in the far-infrared between graphene plasmons and the surface optical phonons of silicon dioxide, ACS Photonics 1 (2014) 1151, https://doi.org/10.1021/ph500233s.
[31] D.V. Smirnov, D.V. Mashovets, S. Pasquier, J. Leotin, P. Puech, G. Landa, Yu.V. Roznovan, Long-wavelength optical phonons of Cd_x $Zn_{1-x}Sb$ mixed crystals, Semicond. Sci. Technol. 9 (1994) 333–337.
[32] P. Nithyadharseni, M.V. Reddy, B. Nalini, M. Kalpana, B.V.R. Chowdari, Sn-based Intermetallic Alloy Anode Materials for the Application of Lithium Ion Batteries, Electrochim. Acta 161 (2015) 261–268, https://doi.org/10.1016/j.electacta.2015.02.057.
[33] Yu M. Basalaev, Ab Initio Study of the $ZnSnSb_2$ Semiconductor, Semiconductors 52 (2018) 1715–1720, https://doi.org/10.1134/S1063782618130043.
[34] Q. Xu, J. Zhou, T.H. Liu, G. Chen, Effect of electron-phonon interaction on lattice thermal conductivity of SiGe alloys, Appl. Phys. Lett. 115 (2019) 023903, , https://doi.org/10.1063/1.5108836.